US 20230182119A1

(19) **United States**

(12) **Patent Application Publication**

Stamenkovic et al.

(10) **Pub. No.: US 2023/0182119 A1**

(43) **Pub. Date: Jun. 15, 2023**

(54) **SCALABLE PT CLUSTER AND RUO2 HETEROJUNCTION ANODE CATALYSTS**

(71) Applicant: **UCHICAGO ARGONNE, LLC**, Chicago, IL (US)

(72) Inventors: **Vojislav Stamenkovic**, Naperville, IL (US); **Rongyue Wang**, Naperville, IL (US); **Dusan Strmcnik**, Woodridge, IL (US)

(73) Assignee: **UCHICAGO ARGONNE, LLC**, Chicago, IL (US)

(21) Appl. No.: **18/104,100**

(22) Filed: **Jan. 31, 2023**

Related U.S. Application Data

(62) Division of application No. 16/584,385, filed on Sep. 26, 2019, now Pat. No. 11,596,928.

Publication Classification

(51) **Int. Cl.**

B01J 23/56	(2006.01)
B01J 37/08	(2006.01)
B01J 37/00	(2006.01)
B01J 37/04	(2006.01)

(52) **U.S. Cl.**

CPC ***B01J 23/56*** (2013.01); ***B01J 37/08*** (2013.01); ***B01J 37/009*** (2013.01); ***B01J 37/04*** (2013.01); *B01J 2523/828* (2013.01); *B01J 2523/821* (2013.01)

(57) **ABSTRACT**

A synthesis process for forming nanodendrites. The nanodendrites are utilized in a process to form a heterojunction catalyst. Nanodendrites may include $PtRu_8$ nanodendrites that can be oxidized through annealing to form $PtRuO_2$. One heterojunction catalyst comprises $PtRuO_2$ on a carbon support.

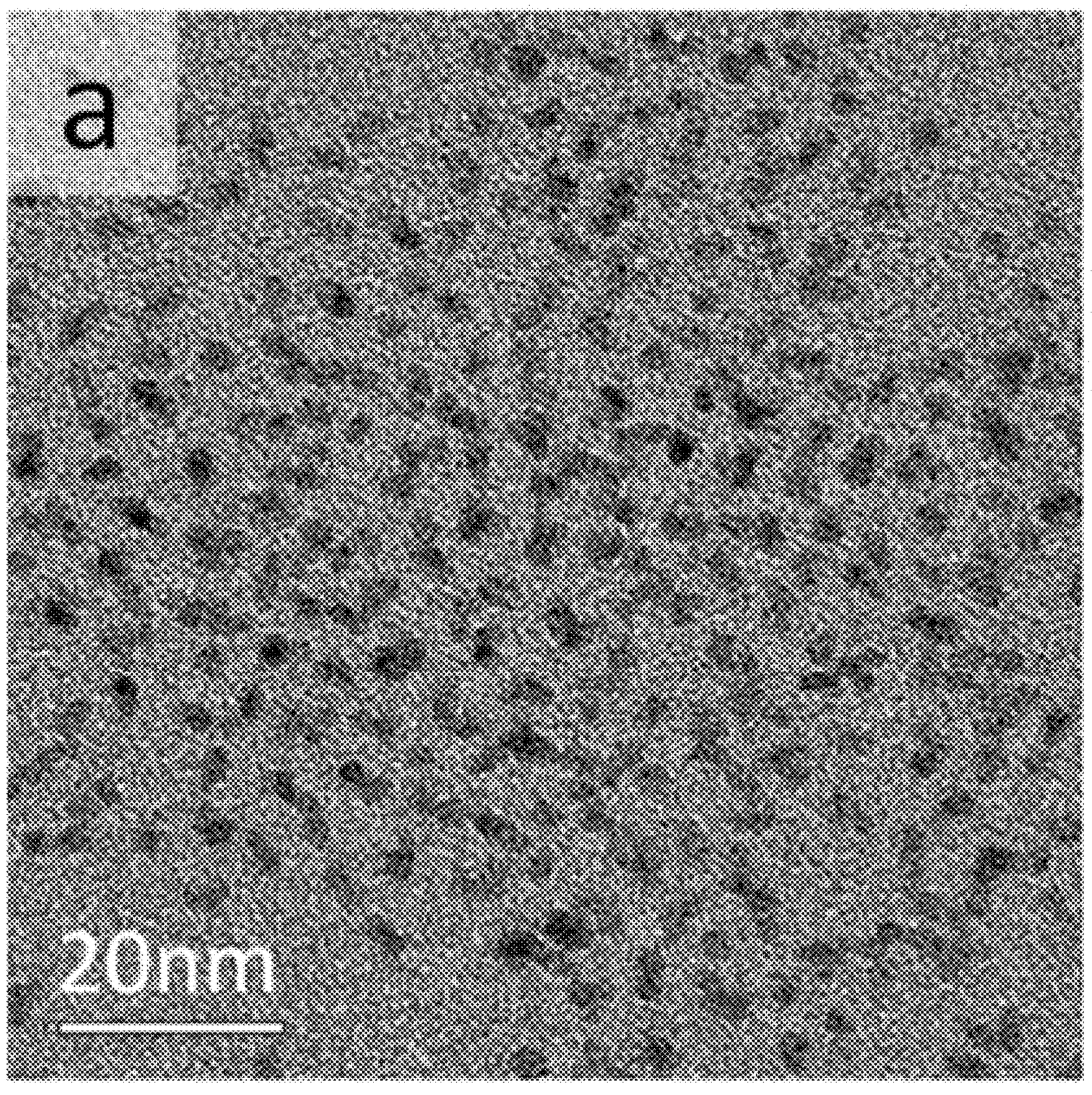

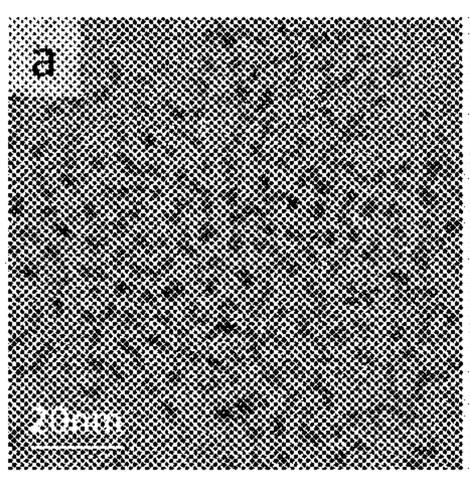

FIG. 1A

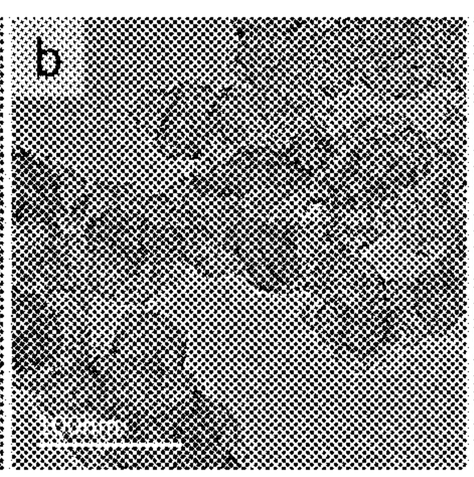

FIG. 1B

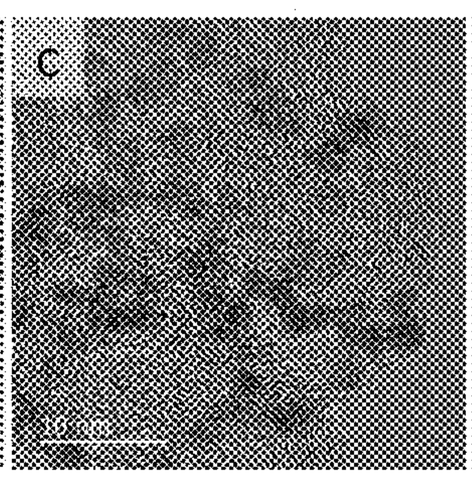

FIG. 1C

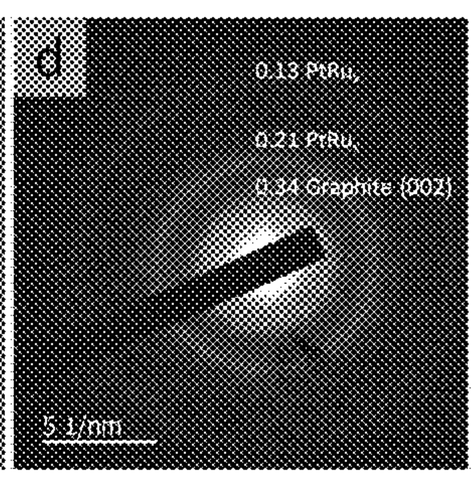

FIG. 1D

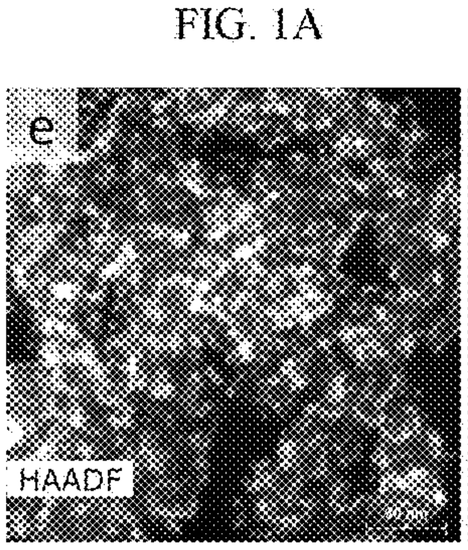

FIG. 1E

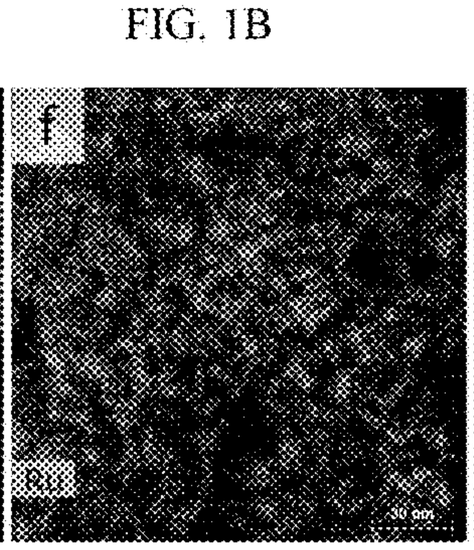

FIG. 1F

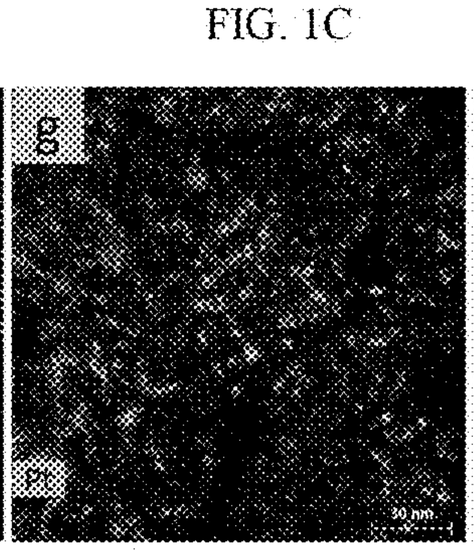

FIG. 1G

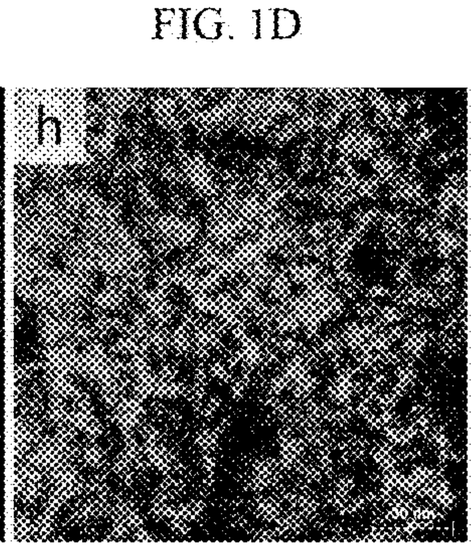

FIG. 1H

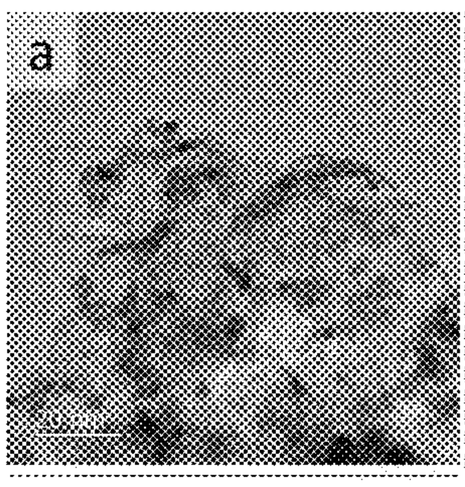

FIG. 2A

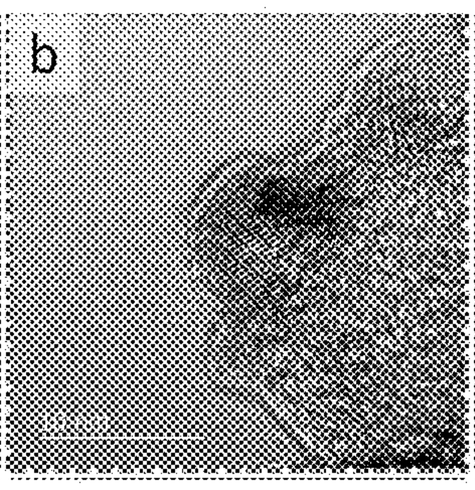

FIG. 2B

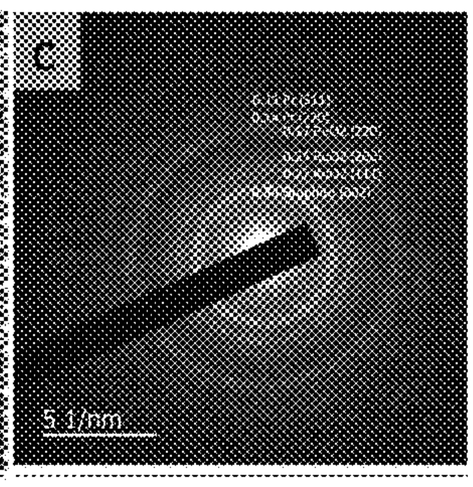

FIG. 2C

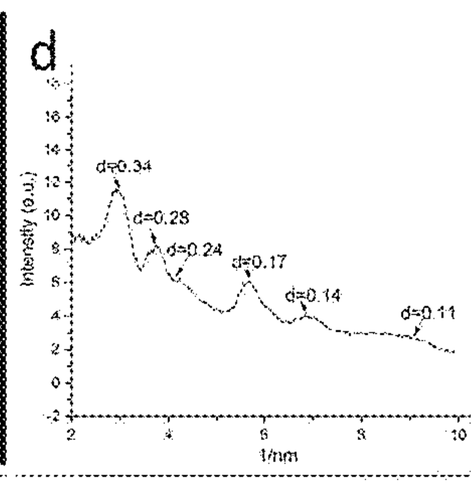

FIG. 2D

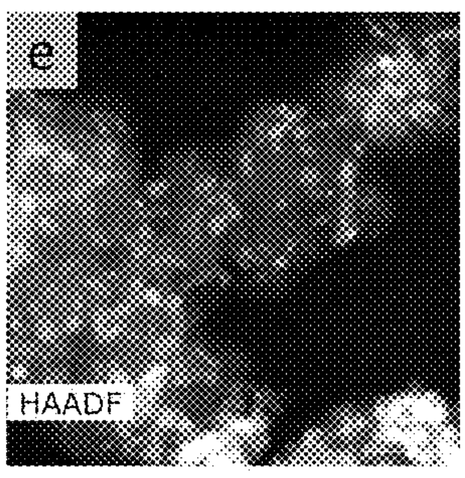

FIG. 2E

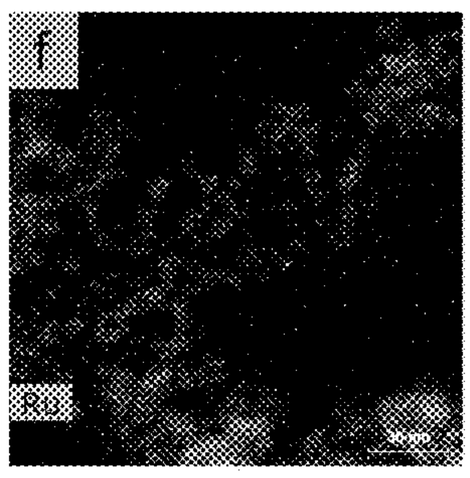

FIG. 2F

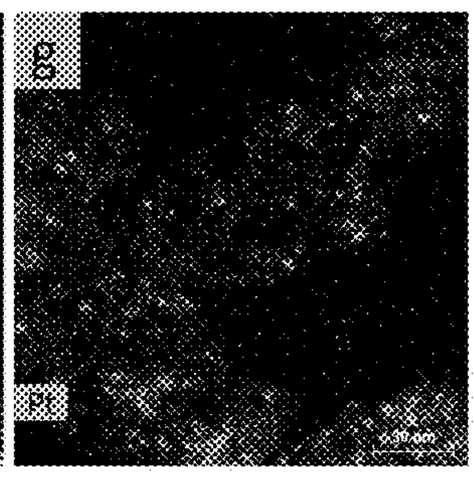

FIG. 2G

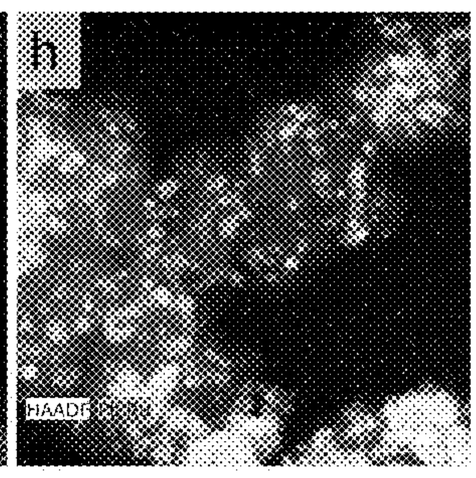

FIG. 2H

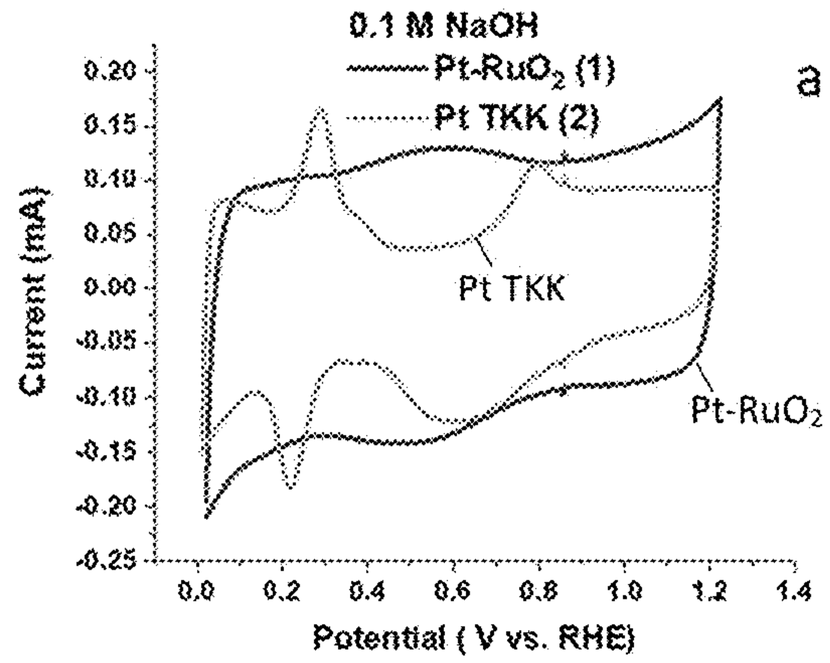

FIG. 3A

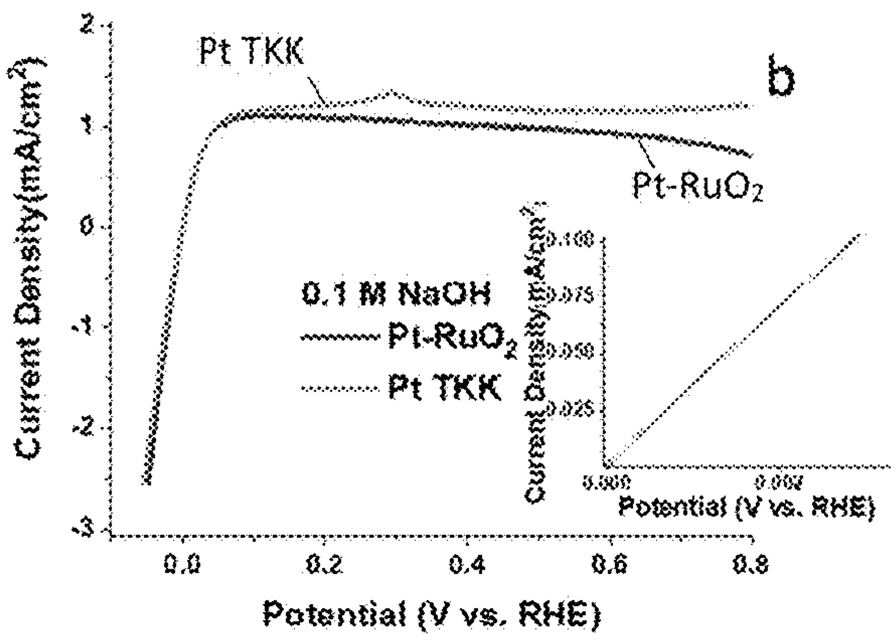

FIG. 3B

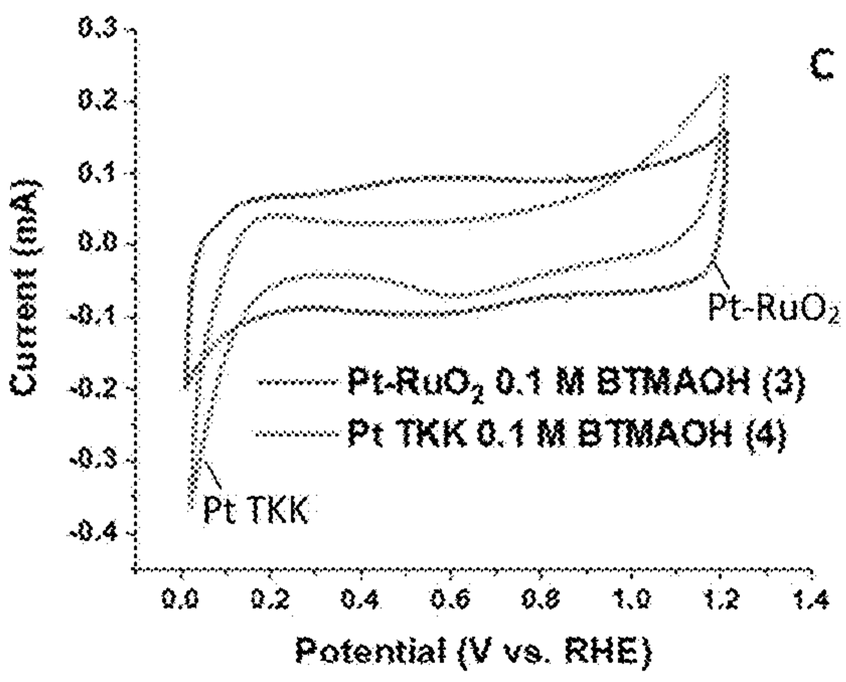

FIG. 3C

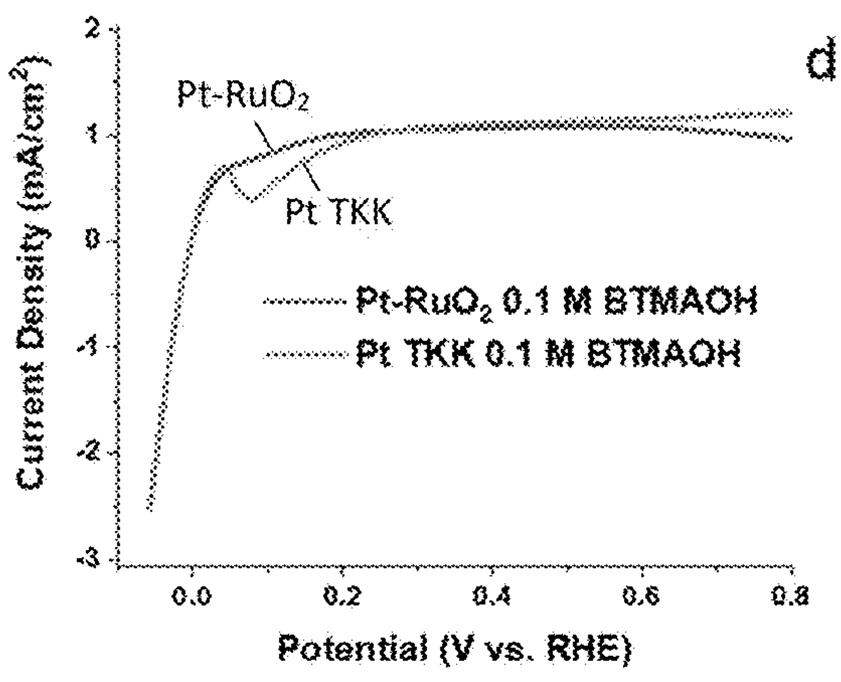

FIG. 3D

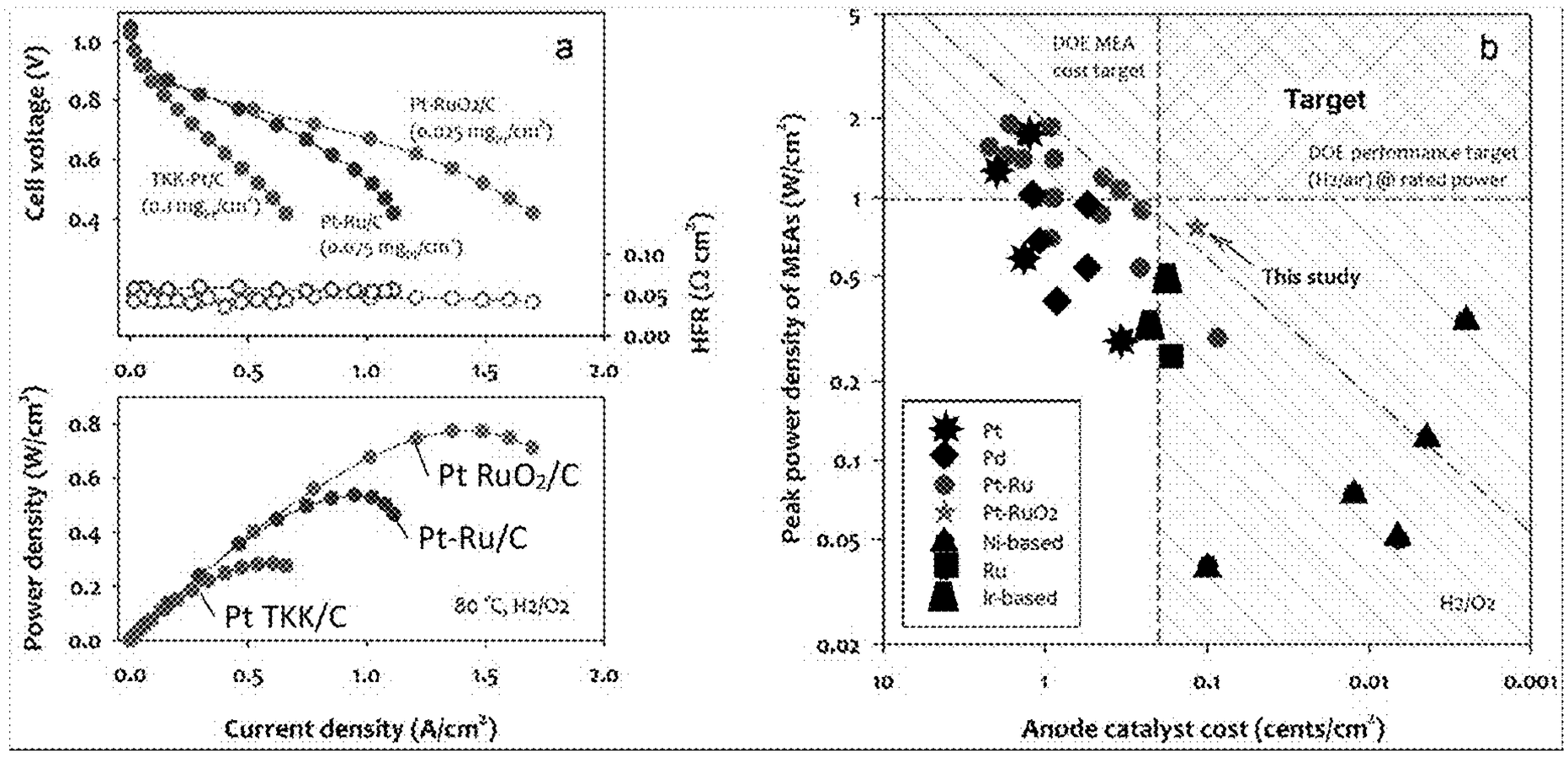

FIG. 4A FIG. 4B

FIG. 5A

FIG. 5B

FIG. 5C

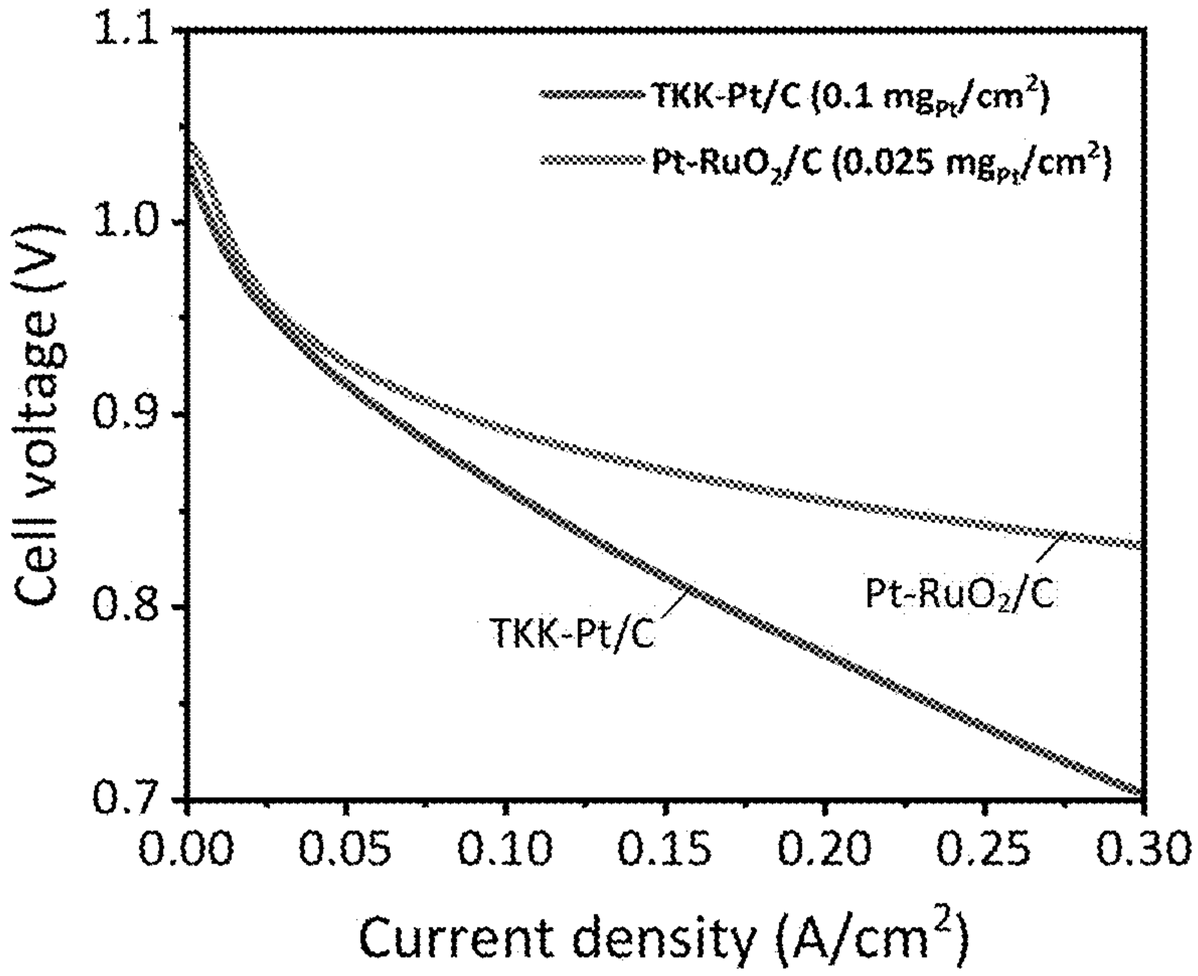
TKK-Pt/C (0.1 mg$_{Pt}$/cm^2)
Pt-RuO$_2$/C (0.025 mg$_{Pt}$/cm^2)
Pt-RuO$_2$/C
TKK-Pt/C
Cell voltage (V)
Current density (A/cm^2)

FIG. 6

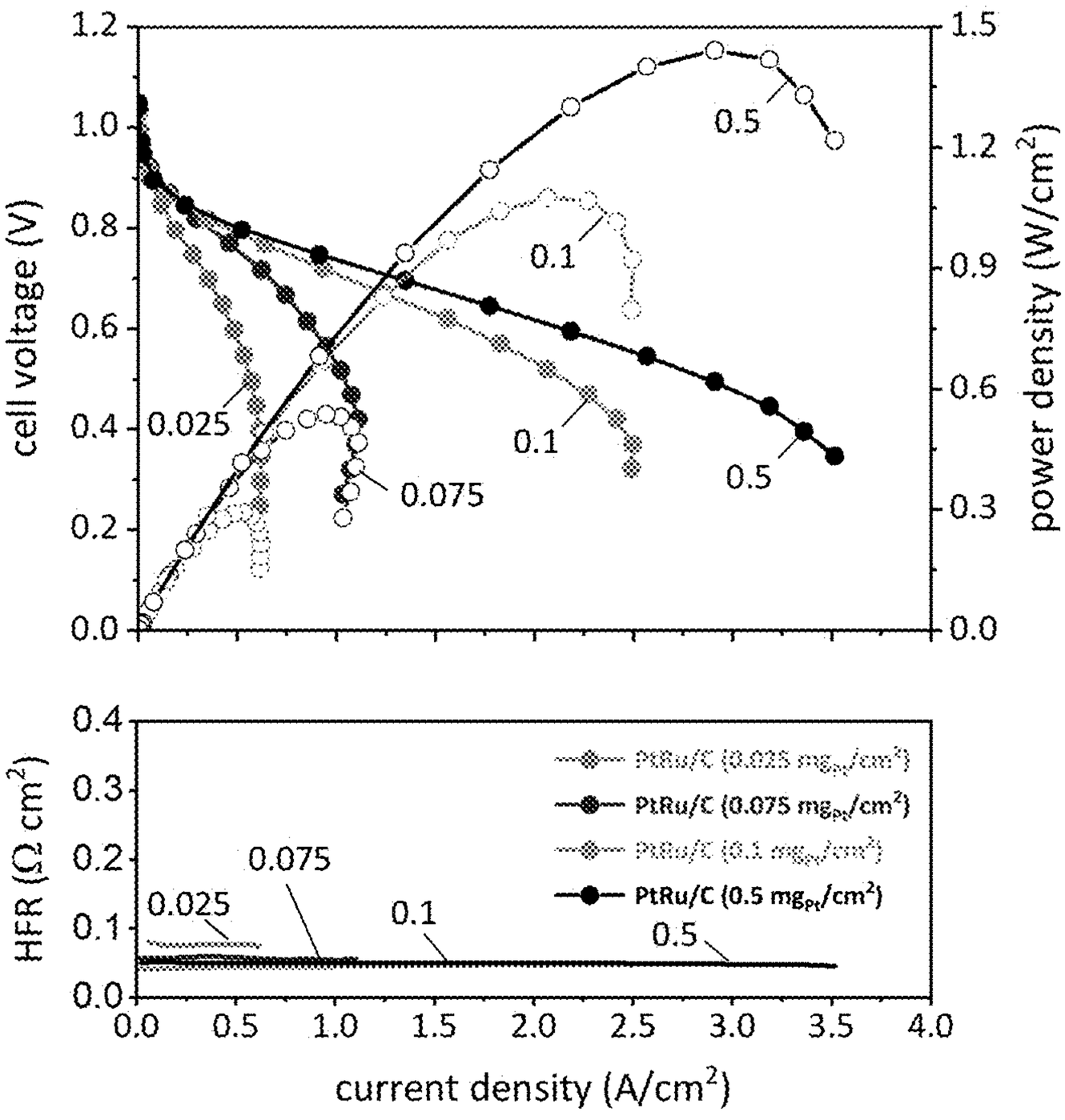
0.5
0.1
0.025
0.075
0.1
0.5
cell voltage (V)
power density (W/cm^2)
PtRu/C (0.075 mg$_{Pt}$/cm^2)
PtRu/C (0.5 mg$_{Pt}$/cm^2)
0.025
0.075
0.1
0.5
HFR (Ω cm^2)
current density (A/cm^2)

FIG. 7

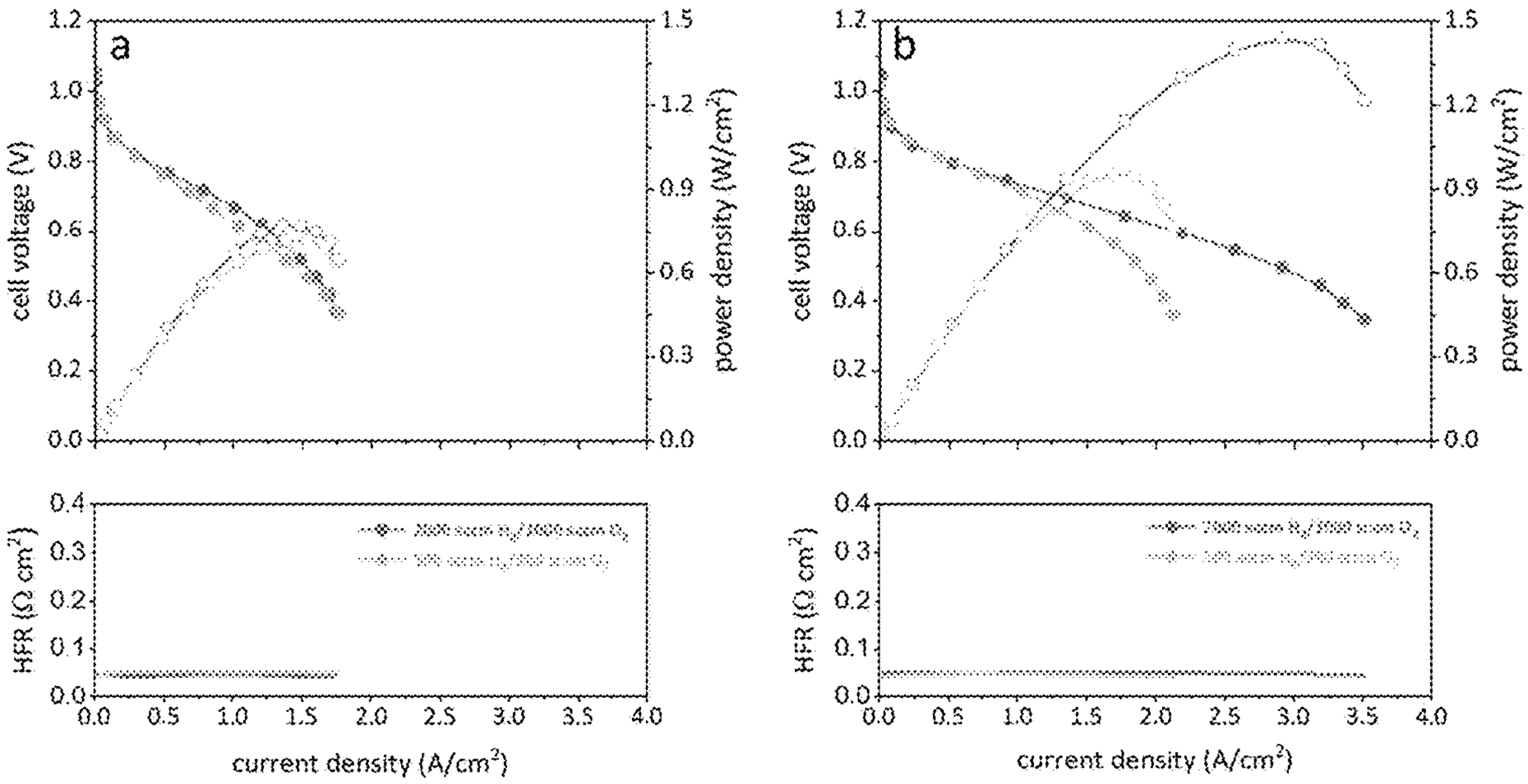

FIG. 8A

FIG. 8B

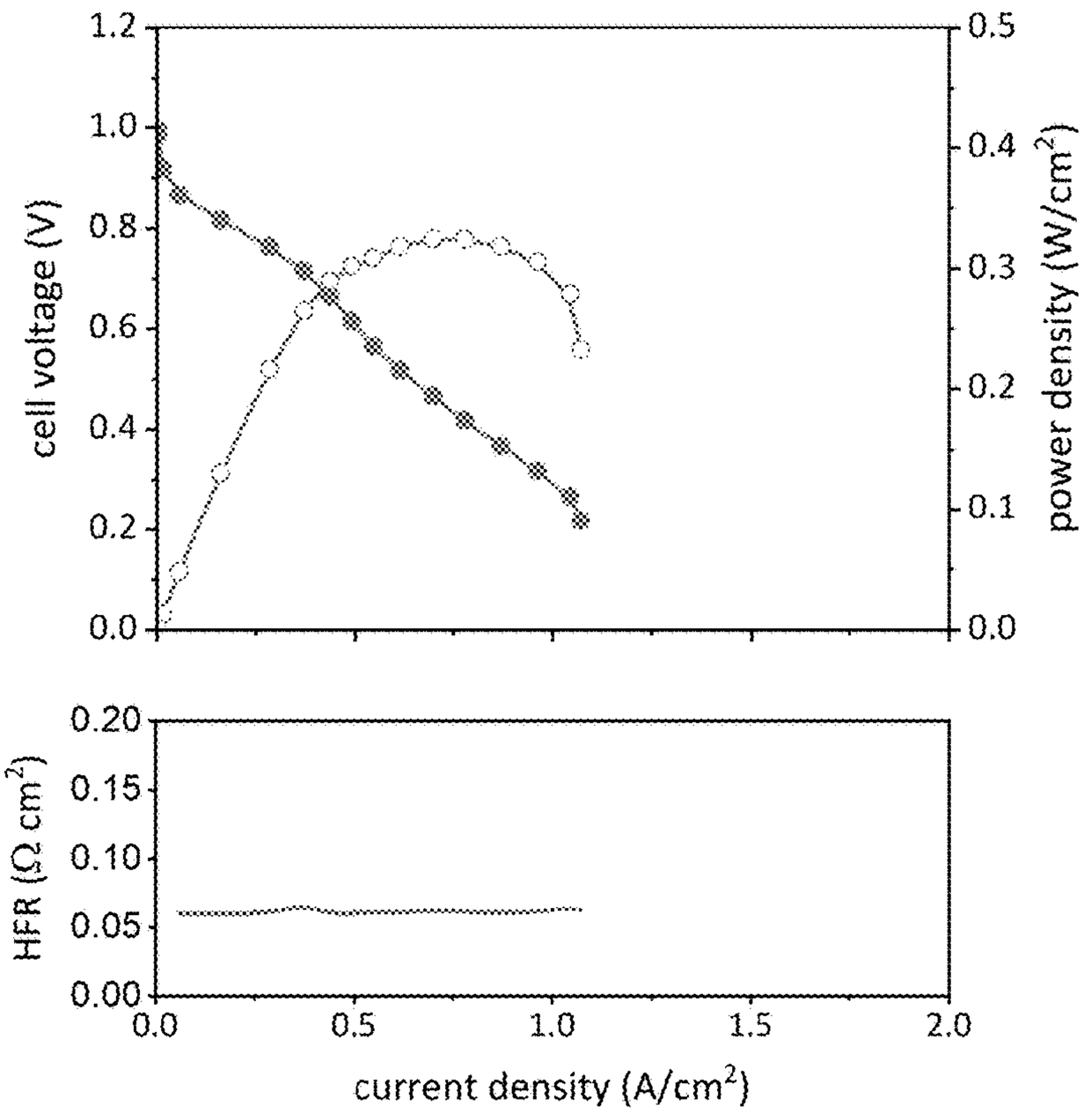

FIG. 9

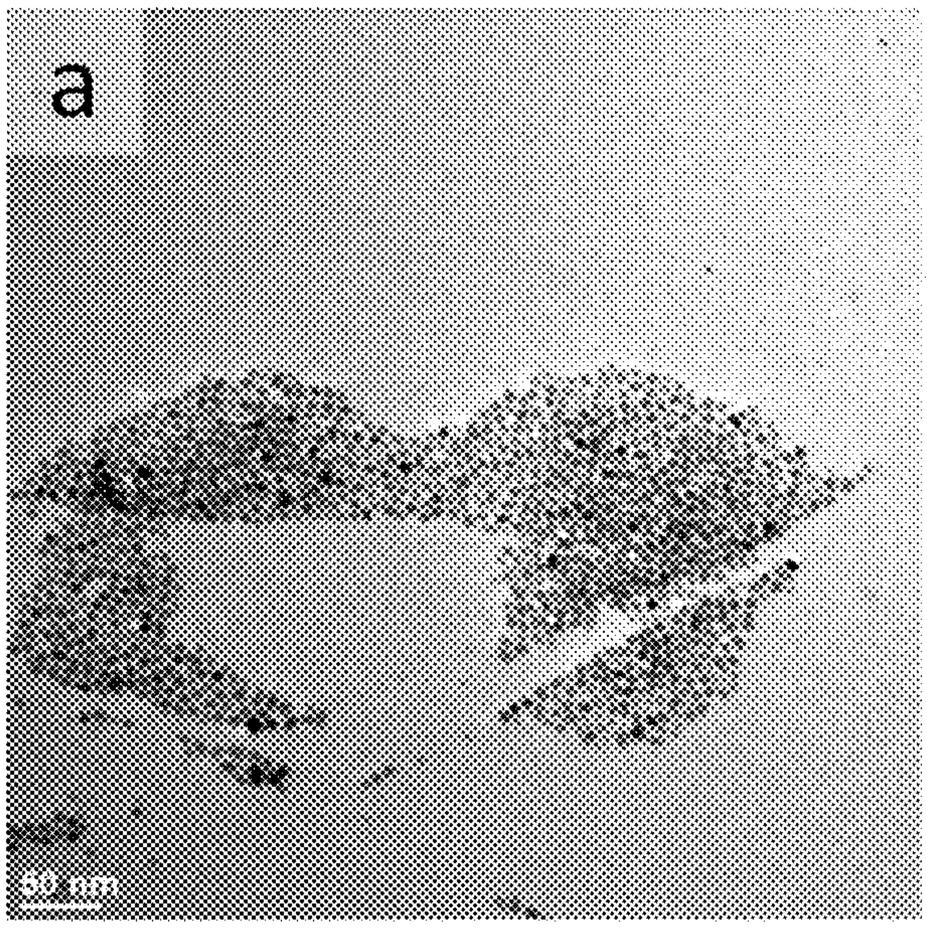

FIG. 10A

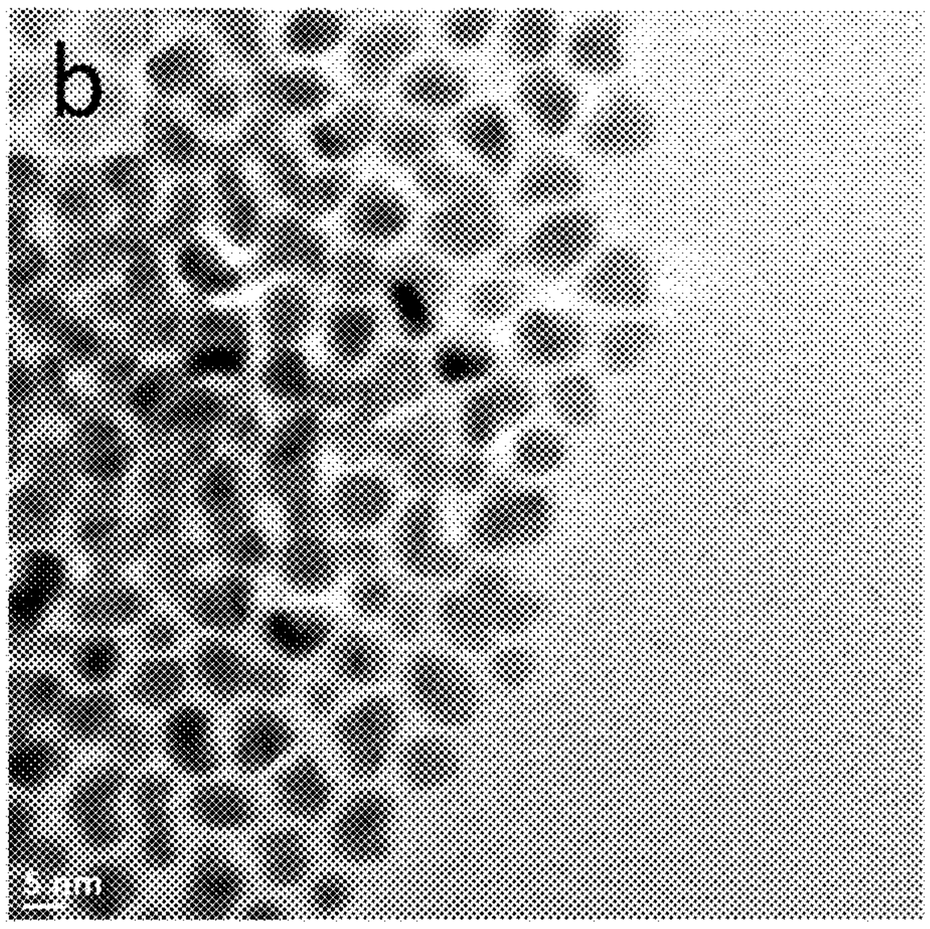

FIG. 10B

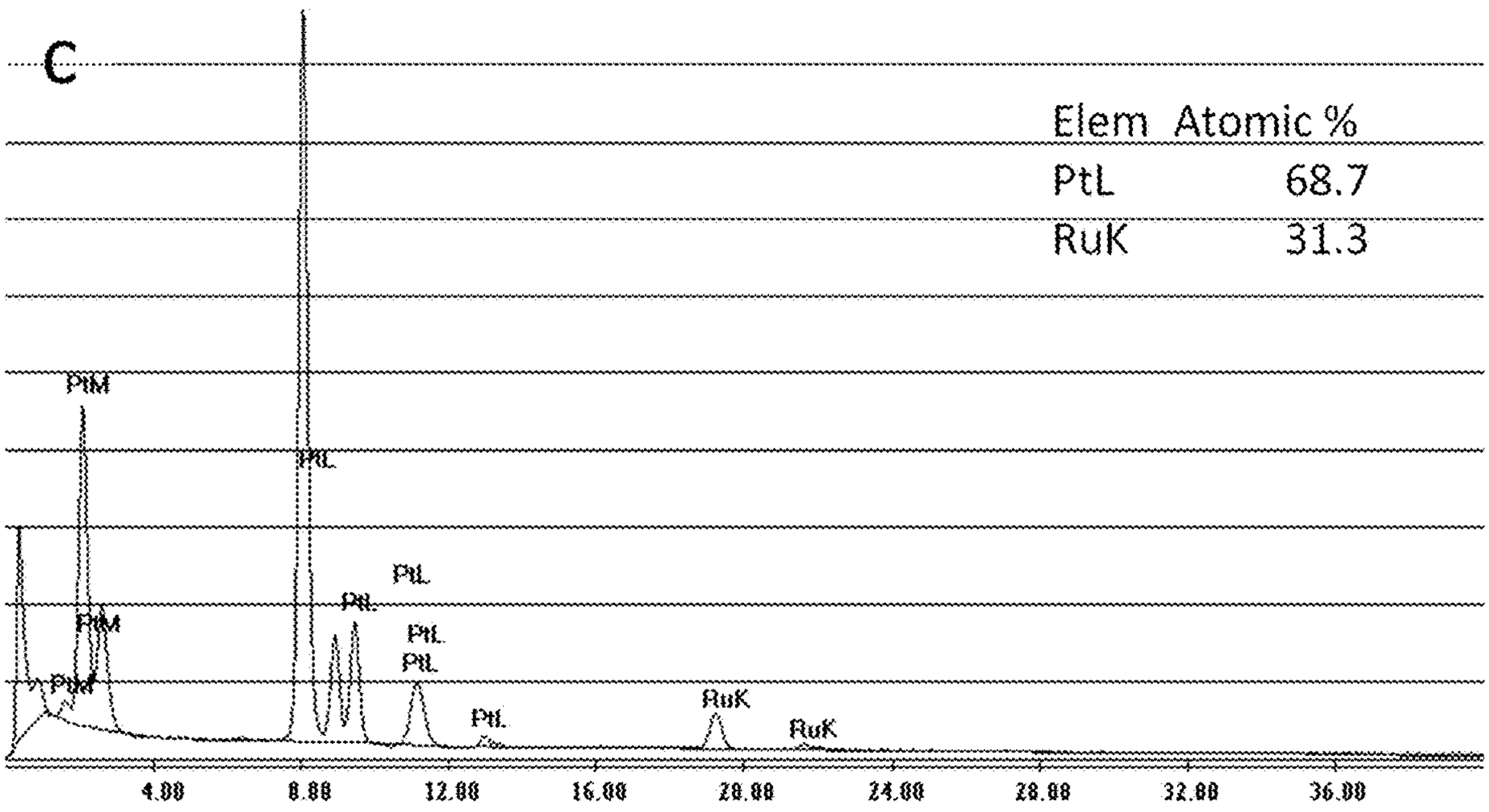

FIG. 10C

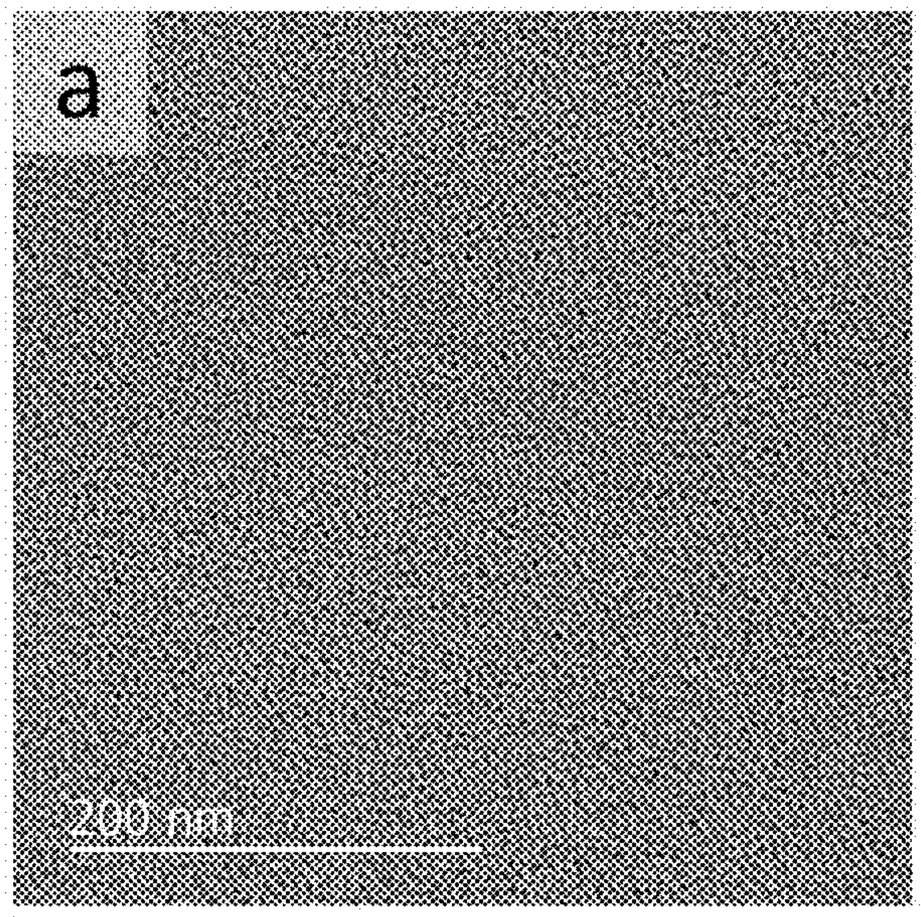

FIG. 11A

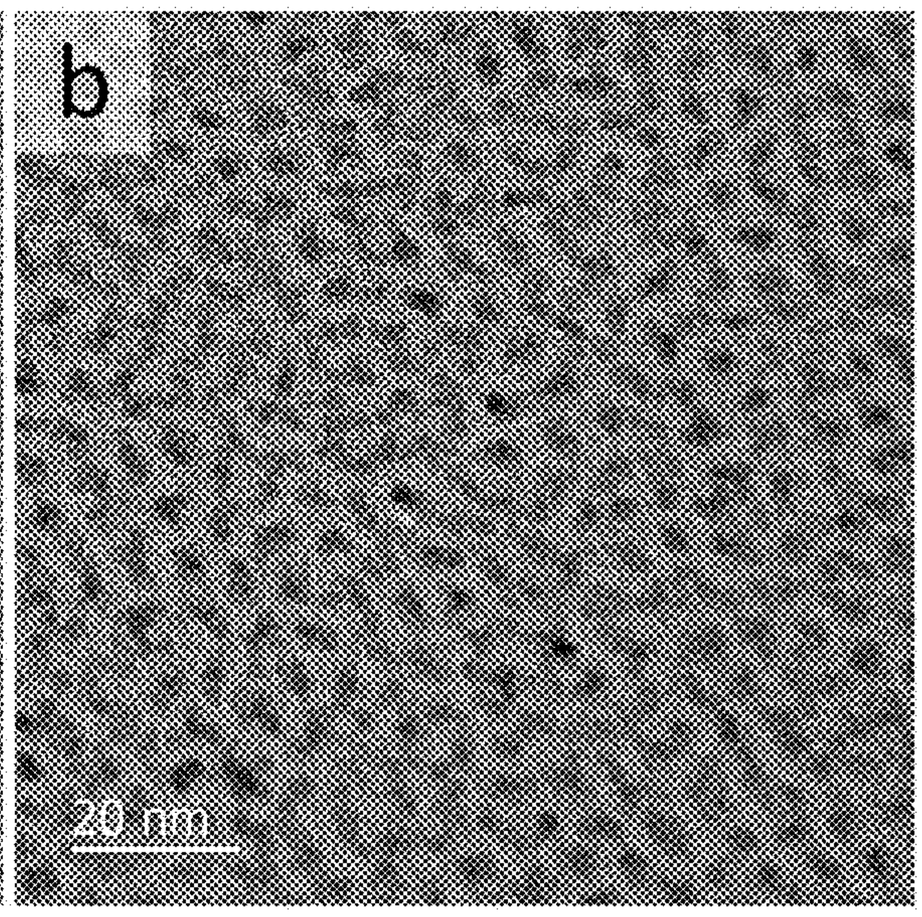

FIG. 11B

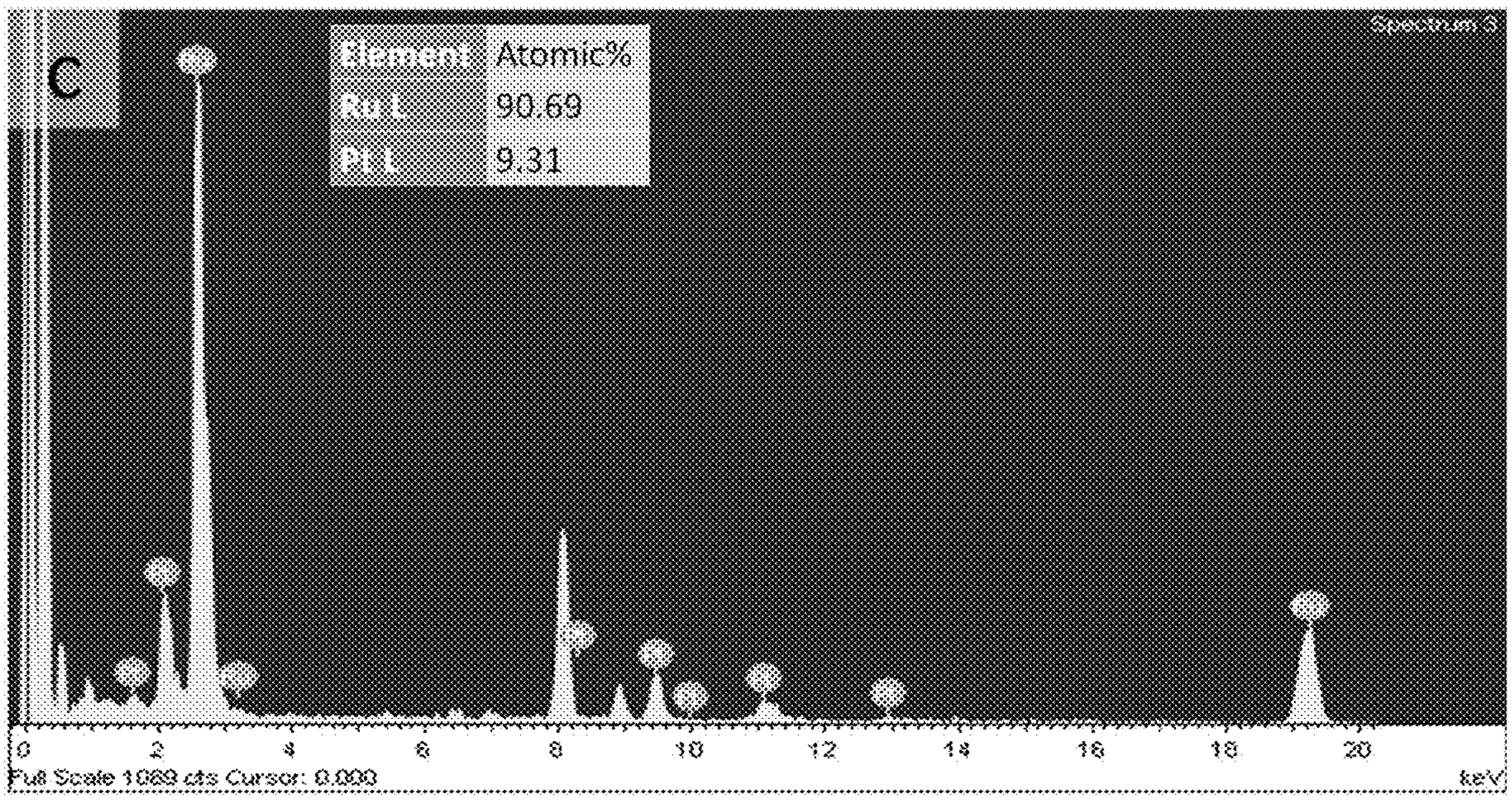

FIG. 11C

SCALABLE PT CLUSTER AND RUO2 HETEROJUNCTION ANODE CATALYSTS

CROSS-REFERENCE TO RELATED APPLICATIONS

[0001] This application is a divisional of U.S. patent application Ser. No. 16/584,385, filed Sep. 26, 2019, the contents of which is incorporated herein by reference in its entirety.

STATEMENT OF GOVERNMENT INTEREST

[0002] This invention was made with government support under Contract No. DE-AC02-06CH11357 awarded by the United States Department of Energy to UChicago Argonne, LLC, operator of Argonne National Laboratory. The government has certain rights in the invention.

TECHNICAL FIELD

[0003] The present disclosure relates to catalytic materials, specifically to heterojunction materials from nanodendrites.

BACKGROUND

[0004] The recent development of novel membranes and ionomers with enhanced hydroxide conductivity and alkaline stability opens up new opportunities for the alkaline anion-exchange membrane fuel cells ("AEMFCs"). However, most of the membrane electrode assemblies ("MEAs") demonstrating high peak power density in literature used a substantial amount of Pt-group metal ("PGM") catalysts for the anode and cathode. Developing cost-effective oxygen reduction reaction ("ORR") catalysts for AEMFCs has been partly successful as the MEAs employing less expensive ORR catalysts showed ~1 W/cm^2 peak power density. However, developing low-cost electrocatalysts for the hydrogen oxidation reaction ("HOR") of the AEMFCs has limited success; therefore, the cost-benefits of AEMFCs over the proton-exchange membrane fuel cells ("PEMFCs") have diminished. Replacing Pt-based HOR catalysts with highly active Pd-based catalysts has become less attractive as the price of Pd is getting higher than that of Pt. Replacing Pt catalysts with non-PGM catalysts has had only limited success because of the relatively low catalytic activity and anode flooding. Reducing Pt loading in the AEMFC anode is a potential solution to reduce the overall cost of AEMFCs. Recently, Omasta, et al., reported ~0.8 W/cm^2 peak power density with a low Pt-loading anode-catalyzed MEA (Anode Pt loading=0.073 mg_{Pt} cm^{-2}).

[0005] To develop highly efficient HOR catalysts for the advanced AEMFC system, not only does the intrinsic kinetic activity of the electrocatalyst need to be taken into account, so too do other parameters, such as compatibility of the catalyst with ionomer of MEA, water management, and the scalability of the catalyst synthetic procedure. Our previous work of HOR on bulk alloy electrode surfaces demonstrated that Pt—Ru bimetallic alloy catalysts have benefits because Ru would provide the sites for OH_{ad}, which can then effectively remove the hydrogen intermediates that are present on the nearby Pt sites. Further, work at Los Alamos National Laboratory found that Pt—Ru bimetallic alloy catalysts also have benefits to minimize the phenyl group adsorption which significantly increases the HOR current density up to 0.5 V vs. reversible hydrogen electrode ("RHE"). Since most ionomeric binders used for the electrolytes of AEMFCs contain phenyl group, the unique low phenyl group adsorbing characteristics of Pt—Ru bimetallic alloy catalysts have shown the dramatic increase in AEMFC power density to ~1.5 W/cm^2 for MEAs using polyaromatic ionomers. Other researchers demonstrated the AEMFC power density of >2.0 W/cm^2 with the MEAs using less phenyl-containing polyolefinic ionomers. Incorporating Ru element to Pt catalyst may significantly reduce the HOR catalyst cost as the Ru price is only ~30% of Pt; however, it is still challenging to maintain the excellent anode performance at low Pt-loading anode with Pt—Ru bimetallic alloys because the water generated from HOR in the thin catalyst layer promotes anode flooding.

SUMMARY

[0006] At least one embodiment relates to a method of forming a $PtRuO_2$ heterojunction catalyst. The method includes forming a solution of platinum precursor, a ruthenium precursor, diphenyl ether, 1,2-tetradecanediol, oleylamine, and dichlorobenzene. The solution is heated to a reaction temperature between 230-270° C. for 5 min-1 h, forming nanodendrites. The nanodendrites are separated from the solution and suspended in organic solvent forming a suspension. The carbon is mixed with the suspension. The carbon material is isolated from the suspension and annealed, converting Ru to RuO_2.

[0007] Another embodiment relates to a method of forming a nanodendrites. The method comprises forming a solution of platinum precursor, a ruthenium precursor, diphenyl ether, 1,2-tetradecanediol, oleylamine, and dichlorobenzene. The solution is heated to a reaction temperature between 230-270° C. for 5 min-1 h. $PtRu_8$ are separated nanodendrites from the solution.

[0008] Yet another embodiment relates to a heterojunction catalyst. The catalyst comprises a carbon substrate and a catalytic material support on the substrate, the catalytic material comprising $PtRuO_2$. The Pt particles have a diameter of 1-5 nm and RuO_2 particles have a diameter of **2-20** nm, the Pt particles and the RuO_2 particles being atomically connected.

[0009] This summary is illustrative only and is not intended to be in any way limiting. Other aspects, inventive features, and advantages of the devices or processes described herein will become apparent in the detailed description set forth herein, taken in conjunction with the accompanying figures, wherein like reference numerals refer to like elements.

BRIEF DESCRIPTION OF THE FIGURES

[0010] FIGS. **1**A-**1**H show transmission electron microscopy ("TEM") characterization of $PtRu_8$ nanodendrites: TEM image of as synthesized nanodendrites (FIG. **1**A), TEM image (FIG. **1**B), high-resolution transmission electron microscopy ("HRTEM") image (FIG. **1**C), select area electron diffraction (FIG. **1**D), high-angle annular dark-field ("HAADF") image (FIG. **1**E), and energy-dispersive X-ray spectroscopy ("EDS") mapping of carbon-supported $PtRu_8$ nanodendrites (FIGS. **1**F-**1**H).

[0011] FIGS. **2**A-**2**H show TEM characterization of Pt—RuO_2 heterojunctions: TEM image (FIG. **2**A), HRTEM image (FIG. **2**B), select area electron diffraction (FIGS.

2C-2D), HAADF image (FIG. 2E), and EDS mapping of Pt—RuO_2 heterojunctions (FIGS. 2F-2H).

[0012] FIGS. 3A-3B show cyclic voltammograms (FIG. 3A) and HOR curves (FIG. 3B) of Pt—RuO_2 and Pt TKK in 0.1 M sodium hydroxide ("NaOH"). FIGS. 3C-3D show cyclic voltammograms (FIG. 3C) and HOR curves (FIG. 3D) of Pt—RuO_2 and Pt TKK in 0.1 M benzyltrimethylammonium hydroxide ("BTMAOH"). Cyclic voltammograms were recorded at 50 mV/s; HOR polarization curves were recorded at 20 mV/s, 900 rpm.

[0013] FIG. 4A shows AEMFC performance comparison between MEAs; anode catalyst: Pt—RuO_2/C, TKK-Pt/C, and JM HiSPEC® 12100 Pt—Ru/C; cathode catalyst: Pt/C (0.6 mg_{Pt}/cm^2). AEMFC performance at 80° C. with humidified H_2 (2000 sccm) and O_2 (1000 sccm) at 285 kPa backpressure. FIG. 4B shows AEMFC peak power density comparison as a function of anode catalyst cost; AEMFC performance was taken from literatures. Anode catalyst cost was calculated from a 5-year average of base metal price.

[0014] FIGS. 5A-5B show TEM images of scale-up Pt—RuO_2 nanoparticles supported on high surface area carbon; FIG. 5C shows the corresponding X-ray diffraction ("XRD") pattern (RuO_2 standard PDF#01-071-48251; Pt standard PDF#01-087-0647).

[0015] FIG. 6 shows a graph of the kinetic performance of Pt/C and Pt—RuO_2/C anode catalyzed MEAs in terms of iR-corrected polarization curves at 80° C. with humidified H_2 (2000 sccm) and O_2 (1000 sccm) at 285 kPa backpressure. Cathode: Pt/C (0.6 mg_{Pt}/cm^2).

[0016] FIG. 7 is a graph of the effect of Pt loading at anode on AEMFC performance. Anode catalyst: JM HiSPEC® 12100 PtRu/C, cathode: JM HiSPEC® 9100 Pt/C (0.6 mg_{Pt}/cm^2). Fuel cells performances were obtained at 80° C. with fully humidified 2000 sccm H_2 and 1000 sccm O_2 at 285 kPa backpressure.

[0017] FIGS. 8A-8B are graphs showing the effect of flow rate on AEMFC performance. FIG. 8A shows Pt—RuO_2/C anode catalyzed MEA, and FIG. 8B shows JM HiSPEC® 12100 Pt—Ru/C anode (0.5 mg_{Pt}/cm^2) catalyzed MEA at 80° C. and 285 kPa backpressure under fully humidified gas feed.

[0018] FIG. 9 is a graph of the AEMFC performance in H_2/CO_2-free air with Pt—RuO_2/C as an anode and Pt/C as a cathode. Fuel cells performances were obtained with fully humidified 2000 sccm H_2 and 1000 sccm CO_2-free air at 285 kPa backpressure.

[0019] FIGS. 10A-10C show TEM images and EDS spectroscopy of PtRu nanoparticles synthesized in dibenzyl ether with oleylamine/oleic acid (0.5 mL each) as surfactants and 1,2-tetradecanediol (84 mg) as reducing agent.

[0020] FIGS. 11A-11C show TEM images and EDX spectroscopy of PtRu nanoparticles synthesized in diphenyl ether with one-pot synthesis.

DETAILED DESCRIPTION

[0021] Before turning to the figures, which illustrate certain exemplary embodiments in detail, it should be understood that the present disclosure is not limited to the details or methodology set forth in the description or illustrated in the figures. It should also be understood that the terminology used herein is for the purpose of description only and should not be regarded as limiting.

[0022] Certain embodiments relate to a Pt—RuO_2 heterojunction catalysts. Such catalysts may be used for cost-effective HOR. Rather than strictly alloying elemental Pt and elemental Ru, one embodiment synthesizes Pt—RuO_2 heterojunction catalysts from $PtRu_8$ nanodendrites.

[0023] One embodiment relates to a method of forming heterojunction catalysts. Specifically, heterojunctions may comprise Pt—RuO_2 catalysts or are other stoichiometric ratios. Further, other elements, such as Ni and Co, may be used rather than Ru.

[0024] The heterojunction catalysts are prepared from nanodendrites; one embodiment uses $PtRu_8$ nanodendrites. In one embodiment, the $PtRu_8$ nanodendrites are formed through a solvothermal synthesis process using an organic solvent, such as diphenyl ether, and an organic reducing agent, such as an organic diol (e.g., 1,2-tetradecanediol), and a surfactant, such as oleylamine, which helps the particle uniformity and size control.

[0025] The metals that form the nanodendrites are supplied via respective precursors, for example platinum precursors and ruthenium precursors In one embodiment, the Pt precursor is platinum (II) acetylacetonate [$Pt(acac)_2$]. In one embodiment, the Ru precursor is ruthenium(III) acetylacetonate [$Ru(acac)_3$]. The ratio of Pt precursor to Ru precursor should be selected to approximate the desired ration in the catalytic material, such as for $PtRu_8$, a ratio of Pt:Ru precursors of 1:12 to 1:6.

[0026] In one embodiment, the nanodendrites are formed through addition of 5-15 mg/ml (e.g., 10 mg/ml) $Ru(acac)_3$, 0.5-1.5 mg/ml (e.g., 1 mg/ml) $Pt(acac)_2$ in diphenyl ether with 0.2-10 mg/ml (e.g., 5 mg/ml) of 1,2-tetradecanediol and 0.01-0.5 ml/ml (e.g., 0.2 ml/ml) oleylamine. These relative amounts may be scaled in some embodiments for a larger reaction batch. The nanodendrite reaction proceeds at a dendrite reaction temperature, such as 230-270° C. (e.g., 260° C.), and a dendrite reaction time, such as 5 min to 1 h. In one embodiment, dichlorobenzene is not injected until the temperature of the solution of 1,2-tetradecanediol and diphenyl reaches 200° C. as it is being heated. In another embodiment, a one pot synthesis approach is utilized with all of the ingredients added and the solution heated to the dendrite reaction temperature.

[0027] $PtRu_8$ nanodendrites are separated from the solvents. In one embodiment, the separation is by centrifuge (10000 rpm for 10 min). The collected nanodendrites are then dispersed in an organic solvent, such as chloroform.

[0028] The collected nanodendrites are then used to form the heterojunction catalyst. The nanodendrites suspended in an organic solvent are mixed with carbon. In one embodiment, the carbon is in the form of carbon nanoparticles, such as 20-100 nm in diameter. In one embodiment, the ratio of carbon to catalytic material (such as $PtRuO_2$) nanodendrites is 50:1 to 3:1. The mixture is agitated, such as by sonication, for a mixing time and then precipitated, such as by addition of hexane.

[0029] The nanodendrite/carbon mixture is annealed to convert the elemental Ru to RuO_2. The annealing step also removes remaining solvent or surfactant. In on embodiment, the annealing is at an annealing temperature within the range of 100-200° C. (e.g., 185° C.) in an ambient air environment. In one embodiment, the annealing is for an annealing time, such as overnight (8-12 hours).

[0030] In one embodiment, the heterojunction catalyst comprises ultrafine Pt particles atomically connected with RuO_2. Ultrafine particles are those below 5 nm, such as 1-5 nm, preferably 2-3 nm. RuO_2 size is not well defined and can

be 3-5 nm to 20 nm. In one embodiment, 2-3 nm (or smaller) Pt is surrounded by 2-3 nm (or smaller) RuO_2. The structure of the catalytic material is a heterojunction with atomically connected interface between Pt and RuO_2.

[0031] Certain embodiments may facilitate a lower electrode loading due to the improved performance properties.

Experimental Results.

[0032] Carbon-supported heterojunction catalysts were prepared by solvothermal synthesis and subsequent thermal treatment. Scale-up synthesis to 1 g/batch yield enables a thorough investigation of its MEA performance in combination with rotating disk electrode ("RDE") studies. The results show a unique morphology with ultrafine Pt particle sizes, and atomically connected interfaces between Pt and RuO_2 provide high catalytic activity toward HOR while maintaining significantly improved H_2 mass transport in MEAs via minimizing undesirable phenyl group adsorption in the polymer electrolyte. The results also demonstrate MEA performance of low anode loading Pt—RuO_2/C with those of the state-of-the-art Pt/C and Pt—Ru/C catalysts.

[0033] In summary, Pt—RuO_2 heterojunction catalyst with ultrafine Pt cluster and atomically connected interface was developed by converting Ru-rich phase of $PtRu_8$ nanodendrite into Pt—RuO_2. The synthetic condition of $PtRu_8$ nanodendrites were investigated and preliminary scale-up was explored. With successful demonstration of one-pot synthesis, further scale-up should be attainable. The Pt—RuO_2 heterojunction catalyst showed excellent catalytic activity towards HOR and significantly lower phenyl group adsorption properties compared with commercial Pt/C catalyst. The AEMFC test suggests that the structure of the Pt—RuO_2 heterojunction catalyst provides high access of H_2 at ultra-low loading anode in combination of the good kinetic activity and less degree of phenyl adsorption, making an ideal low PGM loading catalyst for AEMFCs. This result is the first report that that highly active Pt—Ru bimetallic HOR catalyst can be prepared without alloying Pt and Ru components but providing unique morphology of ultrafine Pt cluster and Pt—RuO_2 heterojunctions.

Synthesis of Pt—RuO_2 Heterojunction Catalysts.

[0034] The Pt—RuO_2 heterojunction catalyst was prepared from PtRu nanodendrites. Several pathways to the PtRu nanoparticles with high surface area were explored using different combinations of solvent, surfactant, and reducing agent. Some of the pathways were seen to produce Pt rich PtRu nanoparticles, while others produced Ru rich PtRu nanoparticles, which are the desired form for the heterojunction catalyst.

Dibenzyl Ether.

[0035] As shown in FIG. **10**A, we found Pt_2Ru_1 nanoparticles of ~5 nm could be made in dibenzyl ether solvent at elevated temperature (FIGS. **10**A-C). Specifically, this pathway used dibenzyl ether with oleylamine/oleic acid (0.5 mL each) as surfactants and 1,2-tetradecanediol (84 mg) as reducing agent. The particles synthesized in dibenzyl ether in the presence of oleic acid is Pt-rich and not uniform because the presence of oleic acid hinders the reduction of Ru precursors; thus, we did not pursue this synthetic route.

[0036] Further, a sample with 1,2-tetradecanediol as a reducing agent resulted in an elemental percentage of PtL 69.7 atomic %, RuK 31.3 atomic %. Without reducing agent, Ru content in the particle is even lower (PtL 85.4 atomic %, RuK 14.6 atomic %), indicating the mild reducing capability of oleylamine is not sufficient to completely reduce Ru precursor under this reaction condition. Even with this modification, the dibenzyl ether route does not provide sufficient Ru content.

Diphenyl Ether.

[0037] Ru-rich nanoparticles with minimal particle size and uniform size distributions could be synthesized in diphenyl ether using 1,2-tetradecanediol and oleylamine. Specifically, experiments for the synthesis of PtRu8 nanodendrite were performed in an Ar flow environment in a round bottom flask. Typically, 0.12 g $Ru(acac)_3$, 2 mL oleylamine, 0.063 g 1,2-tetradecanediol, and 10 mL diphenyl ether were heated up to 260° C. in a round bottom flask with Ar flow and 0.012 g $Pt(acac)_2$ dispersed in 1 mL dichlorobenzene was injected when the temperature of former solution reach 200° C. The mixture was heated up slowly to 260° C. The reaction time was controlled to 20-30 min starting from injection.

[0038] Scale-up synthesis was performed in a bigger round bottom flask with similar synthesis procedure and 6 times higher reaction precursors and reaction volume. Note, severe boiling was observed above 230° C. because the boiling point of dichlorobenzene is only 180° C. Care should be taken on the heating rate to avoid pressure buildup in the flask. Composition of dichlorobenzene could be decreased for larger reaction volume.

[0039] Further, a one-pot synthesis was performed in a similar procedure except that all the reaction precursors were heated up in a round bottom flask. By doing so, we eliminated the hot injection step.

[0040] For those nanodendrites to be used further in formation of the catalyst, the $PtRu_8$ nanodendrites are separated from the solvents by centrifuge (10000 rpm for 10 min). The collected nanodendrites are then dispersed in chloroform for the annealing step.

[0041] Similar particle size and composition were obtained with both 0.5 mL and 2 mL oleylamine as a surfactant and/or slightly changed amount of reducing agent (relative to the prior samples tested) (FIG. **1**A) for which the lower surfactant and reducing agent amount is sufficient for the reaction and further increase does not affect the product significantly. Samples yielded a content of: 0.5 mL surfactant and 84 mg reducing agent (PtL 16 atomic %, RuK 84 atomic %); 2 mL surfactant and 84 mg reducing agent (PtL 14.6 atomic % m RuK 85.4 atomic %); and 2 mL surfactant and 65 mg reducing agent (PtL 16.5 atomic %, RuK 83.5 atomic %).

[0042] The Ru content in the particle is only slightly lower than the precursor ratio, indicating a very high conversion rate of the Ru precursor. As shown in FIG. **1**B, $PtRu_8$ nanodendrites can be loaded onto carbon support uniformly. HRTEM image (FIG. **1**C) and selected area electron diffraction ("SAED") pattern (FIG. **1**D) demonstrated the crystalline nature of the nanodendrites. Although the SAED pattern is weak with ultra-small particle size, HAADF imaging and corresponding EDS mapping revealed that the $PtRu_8$ nanodendrites are composed of Pt-rich core surrounded with Ru-rich branches (FIGS. **1**E-**1**H). From these results, the formation of $PtRu_8$ nanodendrites starts with Pt-rich nuclei because Pt is easier to be reduced than Ru. As the reaction

progresses, $Pt(acac)_2$ is depleted, and Ru-rich branches continue to grow on the surface, leading to the dendrite structure.

[0043] Collected $PtRu_8$ nanodendrites were dispersed in chloroform and were then mixed with proper amount of carbon, which can be calculated from the target PtRu loading on carbon, which was also dispersed in chloroform by sonication. The mixture was sonicated for 20 min and the carbon supported $PtRu_8$ nanodendrites were precipitated with hexane and further separated from solvents by centrifuge. This process also works for scale-up sample preparation; larger amounts of solvents were used to ensure good dispersion of $PtRu_8$ nanodendrites on carbon. The carbon supported $PtRu_8$ nanodendrites were annealed in air at 185° C. overnight to convert elemental Ru into RuO_2 and to remove the surfactant adsorbed on the surface of catalyst.

[0044] Initially synthesis the Pt—RuO_2 heterojunction catalysts on a small scale (0.2 g/batch). Later, a scale-up synthesis of the Pt—RuO_2 heterojunction catalyst was investigated by addressing heat transfer and mass transport challenges. With six times higher volume reaction, the boiling of the reactants above 230° C. is more severe than small batch synthesis because the amount of dichlorobenzene (boiling point=180° C.) is also six times higher while the removal rate of dichlorobenzene by argon flow is limited. The heating rate also decreases as more time is needed for reactants to reach the same reaction temperature. However, similar particle size and composition was obtained with the scale-up synthesis (content 14.1 PtL atomic % and 85.9 RuK atomic %). More importantly, scale-up synthesis is highly reproducible.

[0045] The process of loading $PtRu_8$ nanodendrites on carbon is also scalable. Overall, more than 1 g of Pt—RuO_2/C heterojunction catalyst was obtained by combining the two batch of scale-up synthesis and subsequent annealing in air. Notably, injecting precursors into hot reactive solution (hot-injection) is not favorable for scale-up. Similar particle size and composition were obtained with one-pot synthesis, indicating this newly developed recipe is indeed scalable.

[0046] The Pt—RuO_2 heterojunction catalyst was obtained by annealing of the carbon supported $PtRu_8$ nanodendrites in the air at 185° C. overnight, and Ru was converted into RuO_2. As shown in FIGS. **2**A-**2**H, the uniform dendrite structure was converted into a composite structure with lower contrast due to RuO_2 formation. The HRTEM image in FIG. **2**B and SEAD in FIGS. **2**C-**2**D indicate the formation of Pt—RuO_2 heterojunction structures with atomically connected interfaces. The HAADF imaging and EDS mapping results in FIGS. **2**E-**2**H further demonstrate the Pt—RuO_2 heterojunction structure. Compared with the $PtRu_8$ nanodendrites, the size of the Pt-rich particle is slightly smaller, indicating some of the Ru in these Pt-rich areas is also oxidized and migrated to the RuO_2 region. Also observed was some Pt dispersed in the Ru-rich area, which may be beneficial to the performance at a low-Pt loading AEMFC anode. In some embodiments, during the formation of Ru rich dendrites, there are still Pt precursors left, thus small amount of Pt is observed in Ru rich dendrites.

[0047] ICP-MS confirms that the atomic ratio of Pt:Ru in the heterojunction catalysts prepared from the scale-up synthesis is 1:8. TEM images (FIGS. **5**A-**5**B) showed the six times scale-up Pt—RuO_2 nanoparticles are monodisperse (most particles fall in the range of 3-6 nm in diameter) and are uniformly distributed on high surface area carbon support. XRD pattern also proves that the RuO_2 dominates the particle composition (FIG. **5**C). The carbon supported Pt—RuO_2 heterojunction catalyst from the scale-up synthesis was further investigated in the RDE and AEMFC testing.

Electrochemical Characterization of Pt—RuO_2 Heterojunction Catalysts.

[0048] While RDE test in the acidic electrolyte (mostly perchloric acid and sulfuric acid) has been proved as an efficient technique for the catalyst screening of PENIFCs, a systematic study to compare the RDE results in the alkaline electrolyte with the AEMFC performance is yet to be established. Conventionally, NaOH or KOH electrolyte has been used to reveal the kinetic performance of the catalyst in an RDE setup. Our recent work suggested that this might be insufficient for catalyst screening of AEMFCs, as catalyst/ionomer interactions such as phenyl group adsorption and cation-hydroxide-water co-adsorption could mask the intrinsic kinetic performance of a catalyst. In short, under AEMFC operating conditions, the HOR rate imposes limits on its performance, not to discount the need for continuous improvement of ORR catalysis, which is believed to be facile compared with the sluggish ORR in PENIFC.

[0049] In this work, we carried out the RDE study using two different electrolytes, namely NaOH and BTMAOH, all in 0.1 M solution of Milli-Q water. We first compared the HOR performance by the slope between 0 and 0.1 mA/cm^2 instead of the exchange current density, which is difficult to obtain for nanoscale system. Then, we compared HOR current density at 0.05-0.3 V, which is relevant to the AEMFC operating condition. The results are presented in FIGS. **3**A-**3**D. In NaOH, the TKK Pt/C catalyst shows a typical Pt H_{upd} feature between 0.05 V and 0.40 V. Pt—RuO_2 catalyst shows big capacitance feature in the same potential region, indicating a RuO_2 rich surface (FIG. **3**A). For HOR performance, Pt/C TKK and Pt—RuO_2/C show almost identical kinetic performance near 0 V (FIG. **3**B, inset). Note that with the same metal loading, the synthesized Pt—RuO_2/C catalyst has approximately 3.5% wt. of Pt only, as opposed to the commercial catalyst with 19.4% wt. of Pt. The Pt clusters and their unique heterojunctions with RuO_2 indeed exhibit excellent kinetic performance. When the electrolyte was switched to BTMAOH, TKK Pt/C shows a significant reducing current below 0.2 V, which is likely caused by phenyl group adsorption and subsequent reduction. For Pt—RuO_2, very little current drop is observed, which indicates Pt—RuO_2 interaction with the phenyl group is much weaker than that of pure Pt (FIG. **3**C). In 0.1 M BTMAOH electrolytes, Pt—RuO_2 shows higher current at 0.05-0.3 V, where the catalyst/phenyl group interactions take place (FIG. **3**D). Overall, RDE results suggest that our Pt—RuO_2/C catalyst from the scale-up synthesis has comparable HOR kinetic performance with the commercial Pt/C but higher tolerance of phenyl group poisoning even at significantly lower Pt loading.

Performance of Pt—RuO_2 Heterojunction Catalysts in MEA.

[0050] We evaluated the performance of Pt—RuO_2/C heterojunction and other state-of-the-art Pt-based anode catalysts in MEA. The MEAs tested have the same MEA components except for the anode catalyst. The ionomer to

carbon ("I/C") ratio of the anode was optimized for the best AEMFC performance. FIG. **4**A compares the polarization curve, cell high frequency resistance ("HFR") and power density of the MEAs employing low Pt loading Pt/C, PtRu/C, and Pt—RuO_2/C anode catalysts. Under the H_2/O_2 conditions, the MEA using Pt—RuO_2/C anode catalyst exhibits exceptionally high performance in spite of the lower Pt loading. The peak power density of the MEA using Pt—RuO_2/C anode reached 0.77 W/cm^2, as opposed to the MEA using Pt/C and PtRu/C anode catalysts of which the peak power density was 0.28 and 0.55 W/cm^2, respectively. All MEAs have similar cell HFR (~0.045 W/cm^2), confirming that the different performance is not originated from MEA hydration and catalyst-AEM interface. The kinetic performance difference between the Pt/C and Pt—RuO_2/C catalyzed MEAs is negligible, for example, the iR-corrected current density of the MEAs at 0.95 V are similar (0.026 A/cm^2 for Pt/C vs. 0.028 A/cm^2 for Pt—RuO_2/C) at the similar metal loading (FIG. **6**), while the performance difference became significant as the current density increases. For instance, the current density of the Pt—RuO_2/C catalyzed MEA at 0.85 V is 0.22 A/cm^2, ~2 times of the Pt/C catalyzed MEA. This result is consistent with the RDE experiment where the kinetic activity of Pt—RuO_2/C and Pt/C is comparable, but the overall activity of the Pt/C catalyst is hindered by the adverse adsorption of the phenyl groups of the ionomer. The performance comparison between PtRu/C and Pt—RuO_2/C catalyzed MEAs indicates that the kinetic performance of the MEA using PtRu/C catalysts is slightly higher than that of the MEA using Pt—RuO_2/C (0.036 A/cm^2 for PtRu/C vs. 0.028 A/cm^2 for Pt—RuO_2/C at 0.95 V). However, the performance at the high current density region, ca. >1.0 A/cm^2, the Pt—RuO_2/C catalyzed MEA showed significantly higher performance than the PtRu/C catalyzed MEA.

[0051] The notably higher performance of Pt—RuO_2/C catalyzed MEA could not alone be explained by the phenyl group adsorption since both catalysts have minimal phenyl group adsorption. There are two possible reasons behind the high performance of Pt—RuO_2/C. First, the lower ratio of metal to carbon in electrocatalysts (15% for Pt—RuO_2/C vs. 75% for PtRu/C) increases the electrode thickness which improves the mass transport at the low loading anode. The electrode thickness effect is also apparent in the fuel cell performance as a function of anode PGM loading (FIG. **7**). The peak power density of Pt—RuO_2/C MEA increased only about 20% with 4-times higher anode catalyst loading, while the peak power density of PtRu/C MEA increased ~3.5 times with 4-times higher anode catalyst loading. This indicates that our novel Pt—RuO_2/C heterojunction catalyst works really well for low PGM loading electrodes, on the other hand, the commercial PtRu/C catalysts with high metal content only perform well at higher PGM loadings. Second, the ultrafine Pt clusters surrounded by large RuO_2 particles create desirable morphology for the mass transport. The superior H2 mass transport of the Pt—RuO_2/C at the low loading electrode is also evidenced by the AEMFC performance at reduced H2 flow. The Pt—RuO_2/C catalyzed MEA shows only slightly inferior performance of 0.72 W/cm^2 at a much lower flow rate, while more significant performance loss is observed for the PtRu/C catalyzed MEA (FIGS. **8**A-**8**B). The Pt—RuO_2/C MEA shows the peak power density of 0.33 W/cm^2 at 0.48 V, achieving the specific power (13.2 W/mg$_{Pt}$) under H_2/CO_2-free air conditions (FIG. **9**).

[0052] We further compare the reported AEMFC performance as a function of the cost of anode catalyst. For this analysis, we collected the peak power density of AEMFCs using state-of-the-art anode catalysts in literature and compared the AEMFC performance normalized for anode catalyst cost per cm^2 area based on the 5 year average price of metals. FIG. **4**B plots the peak power density of the MEAs as a function of anode catalyst cost with two target lines (i.e., 2020 US DOE MEA cost target (0.2 cents/cm^2) and the rated performance at rated power (1 W/cm^2) under H_2/air conditions. FIG. **4**B shows that Pt—Ru alloy catalysts have better performance than Pt-, Pd-, Ru-, and Ir-based catalysts at a given catalyst cost. Among the Pt—Ru alloy catalysts shown, four catalysts are located on the upper-performance-cost limit (red dashed line). Those catalysts are the commercial PtRu HiSPEC® 10000 (Pt nominally 40 wt. %, Ru nominally 20 wt. %) supported on Vulcan XC—72R carbon. Two Ni-based non-PGM catalysts are located on or even beyond the upper-performance-cost limit. However, their cell performance needs to improve to reach the DOE performance target. The Pt—RuO_2 heterojunction catalyst we prepared from this work is also located beyond the upper-performance-cost limit, suggesting that the formation of ultrafine Pt cluster with Pt—Ru heterojunction is a promising approach to meet fuel cell cost and performance targets for transportation application. Further optimization of catalyst composition and morphology of the heterojunction catalysts with developing non-PGM ORR catalysts may need for advanced AEMFC systems.

Physical Characterization

[0053] The TEM images were obtained on an FEI Tecnai F20 and JEM-2100F microscopes with accelerating voltage at 300 and 200 kV, respectively. Selected area electron diffraction patterns and EDS results were recorded with JEM-2100F microscope equipped with an Oxford EDS detector. HAADF images and energy dispersive X spectroscopy mapping were recorded on a FEI Talos F200X scanning transmission electron microscope ("STEM") with an accelerating voltage of 200 kV at the Center for Nanoscale Materials, Argonne National Laboratory. XRD patterns were recorded from a Siemens diffractometer D5000. The ICP results of PtRu sample are 7.4 (Ru):1 (Pt), 7.6:1, and 7.7:1 for 3 runs. It is averaged to 7.6:1 and the sample in the manuscript was denoted to $PtRu_8$.

RDE Study.

[0054] Synthesized Pt—RuO_2/C (17% metal wt. on high surface area carbon, Pt/Ru atomic ratio 1/6) and commercial Pt/C (TKK TEC10E20A, 19.4% Pt wt.) were dispersed in water under untrasonication. The catalyst concentration of both inks was 1.25 mg/mL. The ink was pipetted onto a glassy carbon disk (5 mm in diameter) to make 20 μg/cm^2 metal loading and dried in air at room temperature. 10 μL of Nafion D521 (diluted to 0.1% wt.) was then added on the surface as a binder to keep the catalyst on the glassy carbon.

[0055] A home-made fluorinated ethylene propylene ("FEP") cell was used for electrochemical characterization of the catalyst. 0.1 M aqueous solution of NaOH (99.99% from Sigma Aldrich) and BTMAOH (40% wt. solution in

water from TCI Chemical) were used as electrolyte. A mercury/mercury oxide (Hg/HgO) electrode (Pine) was the reference electrode and a graphite rod (Sigma Aldrich) was the counter electrode. The reference potential was converted to RHE. Cyclic voltammograms were recorded in nitrogen purged electrolyte. Before hydrogen oxidation reaction curves were recorded at 900 rpm, the electrolyte was saturated with hydrogen and the working electrode was subject to 1.40 V for 30 seconds to remove the cation adsorption.

Membrane Electrode Assembly.

[0056] The catalyst inks for anode were formulated using Pt/C (TKK TEC10E20A, 19.4 wt. % Pt), synthesized Pt—RuO_2/C (15% metal loading on TKK carbon support) with alkyl ammonium tethered poly(fluorene) ("FLN") ionomer (5 wt. % in 1:1 solution of isopropanol-ethanol) in 20:80 v/v % water — isopropanol solution. The two sets of anodes were prepared with different Pt loading where I/C ratios were 40% for Pt/C and synthesized Pt—RuO_2/C, respectively. The Pt/C (HiSPEC® 9100, Johnson Matthey Fuel Cells, USA) and FLN ionomer were used for the cathode in all MEAs. For cathodes, Pt loading and I/C ratio were 0.6 mgPt/cm^2 and 42%, respectively. The catalyst ink was brush painted on the BC-29 (gas diffusion layer, 5 cm^2, 270 μm thickness) on the vacuum table at 60° C.

[0057] The quaternized poly(terphenylene) ("TPN") membrane was used as polymer electrolyte. Prepared anode, cathode and membrane were used to fabricate MEA after converting to hydroxide form by immersing in 1 M NaOH solution. The MEA was then placed into the fuel cell hardware (5 cm^2, serpentine flow field) supplied by Fuel Cell Technologies Inc.

Single-Cell Tests.

[0058] The pure hydrogen at 2000 sccm and oxygen or CO_2-free air at 1000 sccm supplied to anode and cathode respectively at 100% relative humidity. All the fuel cell tests were performed at operating temperature of 80° C. The polarization curves were acquired at absolute backpressures of 285 kPa using a fuel cell station (Fuel Cell Technologies Inc., USA). Built-in impedance analyzer was used to measure the HFR while obtaining the polarization curves.

Definitions.

[0059] No claim element herein is to be construed under the provisions of 35 U.S.C. § 112(f), unless the element is expressly recited using the phrase "means for."

[0060] As utilized herein, the terms "approximately," "about," "substantially," and similar terms are intended to have a broad meaning in harmony with the common and accepted usage by those of ordinary skill in the art to which the subject matter of this disclosure pertains. It should be understood by those of skill in the art who review this disclosure that these terms are intended to allow a description of certain features described and claimed without restricting the scope of these features to the precise numerical ranges provided. Accordingly, these terms should be interpreted as indicating that insubstantial or inconsequential modifications or alterations of the subject matter described and claimed are considered to be within the scope of the disclosure as recited in the appended claims.

[0061] It should be noted that the term "exemplary" and variations thereof, as used herein to describe various embodiments, are intended to indicate that such embodiments are possible examples, representations, or illustrations of possible embodiments (and such terms are not intended to connote that such embodiments are necessarily extraordinary or superlative examples).

[0062] The term "coupled" and variations thereof, as used herein, means the joining of two members directly or indirectly to one another. Such joining may be stationary (e.g., permanent or fixed) or moveable (e.g., removable or releasable). Such joining may be achieved with the two members coupled directly to each other, with the two members coupled to each other using a separate intervening member and any additional intermediate members coupled with one another, or with the two members coupled to each other using an intervening member that is integrally formed as a single unitary body with one of the two members. If "coupled" or variations thereof are modified by an additional term (e.g., directly coupled), the generic definition of "coupled" provided above is modified by the plain language meaning of the additional term (e.g., "directly coupled" means the joining of two members without any separate intervening member), resulting in a narrower definition than the generic definition of "coupled" provided above. Such coupling may be mechanical, electrical, or fluidic. For example, circuit A communicably "coupled" to circuit B may signify that the circuit A communicates directly with circuit B (i.e., no intermediary) or communicates indirectly with circuit B (e.g., through one or more intermediaries).

[0063] The term "or," as used herein, is used in its inclusive sense (and not in its exclusive sense) so that when used to connect a list of elements, the term "or" means one, some, or all of the elements in the list. Conjunctive language such as the phrase "at least one of X, Y, and Z," unless specifically stated otherwise, is understood to convey that an element may be either X, Y, Z; X and Y; X and Z; Y and Z; or X, Y, and Z (i.e., any combination of X, Y, and Z). Thus, such conjunctive language is not generally intended to imply that certain embodiments require at least one of X, at least one of Y, and at least one of Z to each be present, unless otherwise indicated.

[0064] References herein to the positions of elements (e.g., "top," "bottom," "above," "below") are merely used to describe the orientation of various elements in the FIGURES. It should be noted that the orientation of various elements may differ according to other exemplary embodiments, and that such variations are intended to be encompassed by the present disclosure.

[0065] Although the figures and description may illustrate a specific order of method steps, the order of such steps may differ from what is depicted and described, unless specified differently above. Also, two or more steps may be performed concurrently or with partial concurrence, unless specified differently above.

What is claimed is:

1. A heterojunction catalyst comprising:

a carbon substrate comprising carbon nanoparticles having a diameter of 20-100 nm; and

a catalytic material supported on the carbon substrate, the catalytic material comprising $PtRuO_2$;

wherein the Pt particles have a diameter of less than 5 nm and the RuO_2 comprises RuO_2 particles have a diameter of 2-20 nm, and

wherein the Pt particles and the RuO_2 particles are atomically connected.

2. The heterojunction catalyst of claim **1**, wherein the carbon substrate and catalytic material is 50:1 to 3:1.

3. The heterojunction catalyst of claim **1**, wherein the Pt particles have a diameter of 1-5 nm.

4. The heterojunction catalyst of claim **3**, wherein the Pt particles have a diameter of 2-3 nm.

4. The heterojunction catalyst of claim **1**, wherein the RuO_2 particles have a diameter of 2-3 nm.

6. The heterojunction catalyst of claim **1**, wherein each Pt particle is surrounded by the RuO_2 particles.

7. The heterojunction catalyst of claim **1**, wherein the $PtRuO_2$ is uniformly distributed on the carbon substrate.

* * * * *